Kinetics of Aquation and Anation of Ruthenium(II) Arene Anticancer Complexes, Acidity and X-ray Structures of Aqua Adducts

Fuyi Wang, Haimei Chen, Simon Parsons, Iain D. H. Oswald, James E. Davidson, and Peter J. Sadler*[a]

Abstract: The aqua adducts of the anticancer complexes $[(\eta^6\text{-X})Ru(en)Cl][PF_6]$ (X = biphenyl (Bip) **1,** X = 5,8,9,10-tetrahydroanthracene (THA) **2,** X = 9,10-dihydroanthracene (DHA) **3;** en = ethylenediamime) were separated by HPLC and characterised by mass spectrometry as the products of hydrolysis in water. The X-ray structures of the aqua complexes $[(\eta^6\text{-X})Ru(en)Y][PF_6]_n$, X = Bip, Y = 0.5 H_2O/0.5 OH, n = 1.5 (**4**), X = THA, Y = 0.5 H_2O/0.5 OH, n = 1.5 (**5A**), X = THA, Y = H_2O, n = 2 (**5B**), and X = DHA, Y = H_2O, n = 2 (**6**), are reported. In complex **4** there is a large propeller twist of 45° of the pendant phenyl ring with respect to the coordinated phenyl ring. Although the THA ligand in **5A** and **5B** is relatively flat, the DHA ring system in **6** is markedly bent (hinge bend ca. 35°) as in the chloro complex **3** (41°). The rates of aquation of **1**–**3** determined by UV/Vis spectroscopy at various ionic strengths and temperatures ($1.23–2.59\times10^{-3}$ s^{-1} at 298 K, I = 0.1 M) are >20× faster than that of cisplatin. The reverse, anation reactions were very rapid on addition of 100 mM NaCl (a similar concentration to that in blood plasma). The aquation and anation reactions were about two times faster for the DHA and THA complexes compared to the biphenyl complex. The hydrolysis reactions appear to occur by an associative pathway. The pK_a values of the aqua adducts were determined by ^{1}H NMR spectroscopy as 7.71 for **4**, 8.01 for **5** and 7.89 for **6**. At physiologically-relevant concentrations (0.5–5 μM) and temperature (310 K), the complexes will exist in blood plasma as >89% chloro complex, whereas in the cell nucleus significant amounts (45–65%) of the more reactive aqua adducts would be formed together with smaller amounts of the hydroxo complexes (9–25%, pH 7.4, $[Cl^-]$ = 4 mM).

Keywords: anticancer agents · hydrolysis · kinetics · organometallic compounds · ruthenium

Introduction

Recently we have shown that Ru^{II} arene complexes of the type $[(\eta^6\text{-arene})Ru(XY)(Z)]$, where XY is a chelating diamine such as ethylenediamine (en), and Z is a leaving group such as Cl^-, are cytotoxic to cancer cells including cisplatin-resistant cell lines.[1,2] The cytotoxicity increases with the size of the arene ring system[2] in the series arene = benzene < *p*-cymene < biphenyl < dihydroanthracene < tetrahydroanthracene with X = Cl and PF_6 as counteranion. Other groups have reported anticancer activity for certain phosphino[3] and aminoacidato[4] Ru^{II} arene complexes. The stable water-soluble complex $[(\eta^6\text{-biphenyl})Ru(en)Cl][PF_6]$ (**1**) is active in the A2780 human ovarian cancer xenograft and non-cross-resistant in the A2780cis xenograft.[2]

Since DNA is a potential target for ethylenediamine Ru^{II} arene complexes, we have investigated interactions with nucleotides. The arene complexes exhibit a high selectivity for N7 of guanine and, in contrast to *cis*-$[PtCl_2(NH_3)_2]$, cisplatin, show little binding to adenine.[5] Reactions of the chloro Ru^{II} arene ethylenediamine complexes with nucleotides appear to involve initial aquation of the arene complexes, and reactions of the aqua complexes with cyclic guanosine monophosphate are much faster (ca. 3×) than those of the chloro complexes.[5] However, reactions of the aqua complexes were retarded at high pH (e.g. 9) suggesting that Ru–OH bonds may be less reactive than Ru–OH_2 bonds. Such behaviour appears to parallel that of Pt^{II} diam(m)ine anticancer complexes.[6]

In view of the potential importance of aquation in the biological mechanism of action of these Ru^{II} arene anticancer complexes, we have made detailed studies of the rates of aquation and anation of the series of complexes $[(\eta^6\text{-Bip})$-

[a] Professor Dr. P. J. Sadler, Dr. F. Wang, H. Chen, Dr. S. Parsons, I. D. H. Oswald, J. E. Davidson
School of Chemistry, University of Edinburgh
West Mains Road, Edinburgh EH9 3JJ (UK)
Fax: (+44) 131-650-6452
E-mail: p.j.sadler@ed.ac.uk

Supporting information for this article is available on the WWW under http://www.chemeurj.org/ or from the author. Additional details for X-ray crystallography (Tables S1–S2, Figure S1 and S2), ESI-MS analysis (Figure S3) and kinetic studies (Table S3, Figures S4–S10) as indicated in the text are available.

DOI: 10.1002/chem.200304724

Ru(en)Cl][PF_6] (**1**), [(η^6-THA)Ru(en)Cl][PF_6] (**2**) and [(η^6-DHA)Ru(en)Cl][PF_6] (**3**), where en = ethylenediamine, Bip = biphenyl, THA = 5,8,9,10-tetrahydroanthracene and DHA = 9,10-dihydroanthracene, using HPLC, MS, UV/Vis and NMR spectroscopy (Scheme 1). Complexes **1**–**3** are all

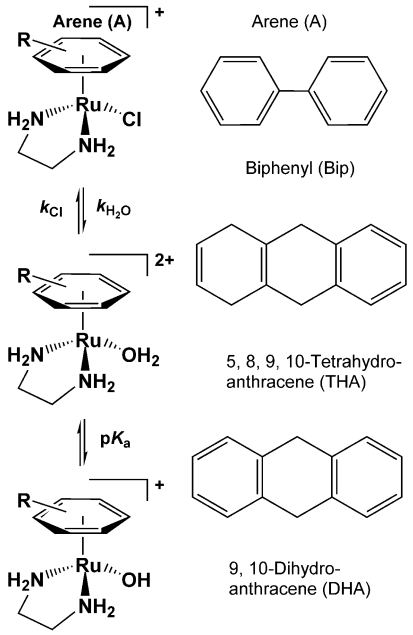

Scheme 1. Hydrolysis and deprotonation of ruthenium arene anticancer complexes.

cytotoxic towards A2780 cancer cells,[2] with a potency order **2** > **3** > **1**. We have determined the acid dissociation constants of the aqua adducts (pK_a) and their X-ray crystal structures. Finally we consider the implications of these findings for the mechanism of biological action.

Results

X-ray structures of aqua ruthenium arene complexes: Crystallographic data for aqua ruthenium arene complexes **4**–**6** are listed in Table 1, and selected bond lengths and angles in Table 2 and Table S1 in the Supporting Information. A comparison of the configurations of the aqua complexes and those of their parent chloro complexes **1**–**3** is given in Table 3. For the biphenyl complex **4**, the X-ray data for one single crystal showed that it could be formulated as a mixed aqua/hydroxo complex [(η^6-Bip)-Ru(en)$(H_2O)_{0.5}(OH)_{0.5}$][PF_6]$_{1.5}$. For the tetrahydroanthracene complex **5**, two single crystals from the same batch were selected for X-ray determination. One crystal could also be formulated as an aqua/hydroxo complex [(η^6-THA)Ru(en)-$(H_2O)_{0.5}(OH)_{0.5}$][PF_6]$_{1.5}$ (**5A**), whereas the second crystal consisted of the aqua complex only, [(η^6-THA)Ru(en)-(H_2O)][PF_6]$_2$·H_2O (**5B**). In **5B** the coordinated OH_2 was disordered and placed at two positions (see Figure S1 in the Supporting Information). For the dihydroanthracene complex **6**, the crystal corresponded to [(η^6-DHA)Ru(en)(H_2O)][PF_6]$_2$·2H_2O and contained only the aqua complex.

In the Bip complex **4** (Figure 1), the propeller twist of the pendant phenyl ring with respect to the coordinated phenyl ring of the Bip ligand is 45.3°, which is 19.1° larger than that for the chloro complex **1** (Table 3). The long axis

Table 2. Selected bond lengths (Å) and angles (°) for [(η^6-Bip)Ru(en)-$(H_2O)_{0.5}(OH)_{0.5}$][PF_6]$_{1.5}$ (**4**), [(η^6-THA)Ru(en)(H_2O)][PF_6]$_2$·(H_2O) (**5B**) and [(η^6-DHA)Ru(en)(H_2O)][PF_6]$_2$·2(H_2O) (**6a**). For numbering schemes see Figure 1.

	4	**5B**[a]	**6a (Ru1)**[a]
Ru1–O1W	2.090(4)	2.163(5) (O1)[b] 2.163(8) (O1′)[c]	2.161(5) (O1)
Ru1–N1B	2.113(5)	2.111(4)	2.138(7) (N12)
Ru1–N2B	2.130(5)	2.115(5)	2.135(6) (N22)
Ru1–C1A	2.207(6)	2.224(5)	2.235(7) (C11)
Ru1–C2A	2.188(6)	2.180(5)	2.176(7) (C21)
Ru1–C3A	2.164(7)	2.175(5)	2.174(7) (C31)
Ru1–C4A	2.162(7)	2.156(5)	2.164(7) (C41)
Ru1–C5A	2.173(7)	2.146(5)	2.210(7) (C51)
Ru1–C6A	2.201(6)	2.216(5)	2.207(7) (C61)
N1B-Ru1-N2B	79.4(2)	79.44(18)	78.6(3) N12-Ru1-N22
N1B-Ru1-O1W	79.4(2)	77.4(2) (O1)[b] 88.4(4) (O1′)[c]	81.5(2) N12-Ru1-O1
N2B-Ru1-O1W	82.7(2)	87.6(2) (O1)[b] 70.8(4) (O1′)[c]	81.9(2) N22-Ru1-O1

[a] The bond lengths and angles for complex **5A** and cation **6b** are listed in Table S1 in the Supporting Information. [b] With an occupancy factor of 0.7. [c] With an occupancy factor of 0.3.

Table 1. Crystal structure data for [(η^6-Bip)Ru(en)$(H_2O)_{0.5}(OH)_{0.5}$][PF_6]$_{1.5}$ (**4**), [(η^6-THA)Ru(en)-$(H_2O)_{0.5}(OH)_{0.5}$][PF_6]$_{1.5}$ (**5A**), [(η^6-THA)Ru(en)(H_2O)][PF_6]$_2$·(H_2O) (**5B**), and [(η^6-DHA)Ru(en)(H_2O)][PF_6]$_2$·2(H_2O) (**6**).

	4	**5A**	**5B**	**6**
formula	$C_{28}H_{39}F_{18}N_4O_2P_3Ru_2$	$C_{32}H_{47}F_{18}N_4O_2P_3Ru_2$	$C_{16}H_{26}F_{12}N_2O_2P_2Ru$	$C_{16}H_{20}F_{12}N_2O_3P_2Ru$
molar mass	1100.68	1156.79	669.40	685.40
crystal system	monoclinic	orthorhombic	triclinic	triclinic
crystal size [mm]	0.43 × 0.21 × 0.09	0.22 × 0.10 × 0.06	0.28 × 0.24 × 0.18	0.30 × 0.14 × 0.12
space group	*C*2/*c*	*Ibam*	$P\bar{1}$	$P\bar{1}$
crystal	orange	yellow	yellow	orange
a [Å]	14.400(4)	23.313(5)	9.3030(17)	11.586(3)
b [Å]	16.011(5)	12.272(2)	9.8849(18)	13.319(4)
c [Å]	17.049(5)	14.249(3)	13.086(2)	16.241(4)
α [°]	90	90	85.585(3)	98.663(4)
β [°]	106.881(4)	90	88.262(3)	94.970(4)
γ [°]	90	90	85.679(3)	91.094(4)
T [K]	150 (2)	150(2)	150 (2)	150(2)
Z	4	4	2	4
R [$F > 4\sigma(F)$][a]	0.0524	0.0650	0.0562	0.0936[d]
R_w[b]	0.1254	0.1394	0.1409	0.0772[d]
GOF[c]	1.055	1.232	1.034	1.117
$\Delta\rho$ max and min [eÅ^{-3}]	+1.64, −1.12	+0.91, −1.25	+1.31, −1.02	+ 2.28, −1.21

[a] $R = \Sigma||F_o| - |F_c||/\Sigma|F_o|$. [b] $R_w = [\Sigma w(F_o^2 - F_c^2)^2/\Sigma wF_o^2)]^{1/2}$. [c] GOF $= [\Sigma w(F_o^2 - F_c^2)^2/(n-p)]^{1/2}$, where n = number of reflections and p = number of parameters. [d] Refinement based on *F* with 7242 data with $F > 6\sigma(F)$.

Table 3. Comparison of the conformations of aqua Ru arene complexes **4**–**6** (Figure 1) and their parent chloro-complexes[1,19] **1**–**3**. X = H_2O or Cl. Comparison of biphenyl complex **4** (H_2O) and **1** (Cl).

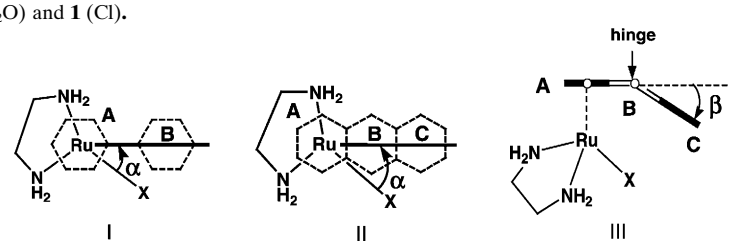

	4 (H_2O)	**1** (Cl)[1]	**5A** (H_2O)	**5B** (H_2O)	**2** (Cl)[19]	**6** (H_2O)		**3** (Cl)[19]
Bip orientation, α (I)	23.3(3)	26.8(2)						
$[\Delta\alpha]$[b] [°]	[−3.5]							
Bip propeller twist, χ[a]	45.3(3)	26.2(4)						
$[\Delta\chi]$[b] [°]	[+19.1]							
Ru-coordinated ring (centroid) [Å]	1.663 (3)	1.663 (3)	1.653(3)	1.664 (2)	1.676(3)	1.671(3)[e]	1.678(3)[f]	1.667(3)
THA/DHA orientation, α (II)			0.00(17)	63.7(2)	45.12(6)	32.5(3)[e]	35.5(3)[f]	64.09(8)
$[\Delta\alpha]$[d] [°]			[−45.12]	[+18.58]		[−31.59]	[−28.6]	
Hinge bending angle, β (III)[c]			+ 11.60	−1.8(3)	−7.53(12)	+31.8(4)[e]	+38.4(4)[f]	+40.65(16)
$[\Delta\chi]$[d] [°]			[−19.13]	[+5.73]		[−8.85]	[−2.25]	

[a] χ: twist of pendant phenyl ring (B) with respect to coordinated phenyl ring (A) of Bip. [b] The change in torsion angle for **4** compared to **1.** [c] The hinge is defined by C7A–C10A, see Figure 1. A + ve sign for β indicates movement towards Ru–X. [d] The change of torsion angles for **5** and **6** compared to **2** and **3**, respectively. [e] Cation **6a**. [f] Cation **6b**.

of Bip is rotated away from the Ru–O vector by 23.3°, which is 3.5° smaller than that for complex **1**. The distance from the Ru centre to the centroid of the coordinated phenyl (A) is 1.66 Å, similar to that in complex **1**.

For the THA complex **5**, the geometry of cation **5A** (see Figure S1 in the Supporting Information) showed high symmetry along a plane through the long axis of the THA ring, Ru1 and O1W atoms. Thus the long axis of THA nearly overlaps with the Ru–O1W vector (Table 3). The outer ring (C) of the THA ligand is slightly bent down towards the O1W atom (hinge bending) by 11.6°. For the cation **5B** (Figure 1b), the coordinated H_2O molecule was disordered over two positions O1 and O1′ with occupancy factors of 0.7 and 0.3, respectively (see Figure S1 in the Supporting Information). The THA tricyclic ring system is nearly flat. The outer ring (C) is slightly bent up away from the O atom (hinge bending) by 1.8°, similar to that in complex **2** (7.5°). The long axis through the THA ligand is rotated away from the major Ru–O vector by 63.7°, which is 18.6° larger than in complex **2**. The distance from Ru to the centroid of coordinated ring (A) is 1.66 Å, similar to that in complex **2**.

For the DHA complex **6**, there are two kinds of independent cations (two **6a** cations, Figure 1c and two **6b** cations, see Figure S2 in the Supporting Information) in the asymmetric unit, and two water solvent molecules. The structures of these two cations **6a** and **6b** differ significantly only in the orientation and hinge bending of the DHA ring. The outer ring (C) is bent down towards the O atom by 31.8° in cation **6a** and by 38.4° in cation **6b**, comparable to that in complex **3** (40.6°). The long axis through the DHA ligand is rotated away from the Ru–O vector by 32.5° in cation **6a** and by 35.5° in cation **6b**, values which are about 30° smaller than that in complex **3** (Table 3). The distance from the Ru atom to the centroid of the coordinated ring (A) is 1.67 Å in both **6a** and **6b**, similar to that in complex **3**. There is an interesting chain of intermolecular hydrogen bonds O4···O1···O3···O5···O2···O6 involving the coordinated and solvent water molecules, and en NH···O4/O6 hydrogen bonding contributes to the crystal packing of both cations **6a** and **6b** (see Figure S2 in the Supporting Information).

HPLC separation and ESI-MS identification of hydrolysis products: Aqueous solutions of the chloro complexes [(η^6-Bip)Ru(en)Cl][PF_6] (**1**), [(η^6-THA)Ru(en)Cl][PF_6] (**2**) or [(η^6-DHA)Ru(en)Cl][PF_6] (**3**) were allowed to equilibrate for 12 h at ambient temperature and were then analysed by HPLC. Two well-separated peaks were observed for each complex (Figure 2), which were identified by the subsequent ESI-MS assays. The observed positive ions are listed in Table 4, and mass spectra are shown in Figure S3 in the Supporting Information.

The seven isotopes of ruthenium give rise to a characteristic pattern in the mass spectra of ruthenium complexes.[7] The first HPLC fraction (retention time: 5.03 min) from complex **1** in aqueous solution gave rise to two ion peaks at *m/z* 314.8 and 428.9 assignable on the basis of mass-to-charge ratios and isotopic models (see Figure S3a in the Supporting Information) to the aqua complex [(η^6-Bip)-Ru(en)(H_2O)]$^{2+}$ (**4**$^{2+}$) (calcd *m/z* 315.0 for [**4**$^{2+}$−H_2O−H]$^+$) and its TFA adduct (calcd *m/z* 429.0 for [**4**$^{2+}$−H_2O+TFA]$^+$), respectively. The second HPLC fraction (9.61 min) gave a peak at *m/z* 350.9 corresponding to the intact cation of **1** (calcd 351.0 for **1**$^+$). Analogous products in aqueous equilibrium solutions of complexes **2** and **3** were also identified by ESI-MS analysis of their HPLC fractions (see Figures S3b and S3c in the Supporting Information).

pK_a determinations: Complexes **4**, **5** and **6** all give rise to two ^{1}H NMR resonances assignable to the two non-equivalent NH protons on each NH_2 group of coordinated en (NH_d protons are oriented away from the coordinated arene, and NH_u towards the coordinated arene). As the pH

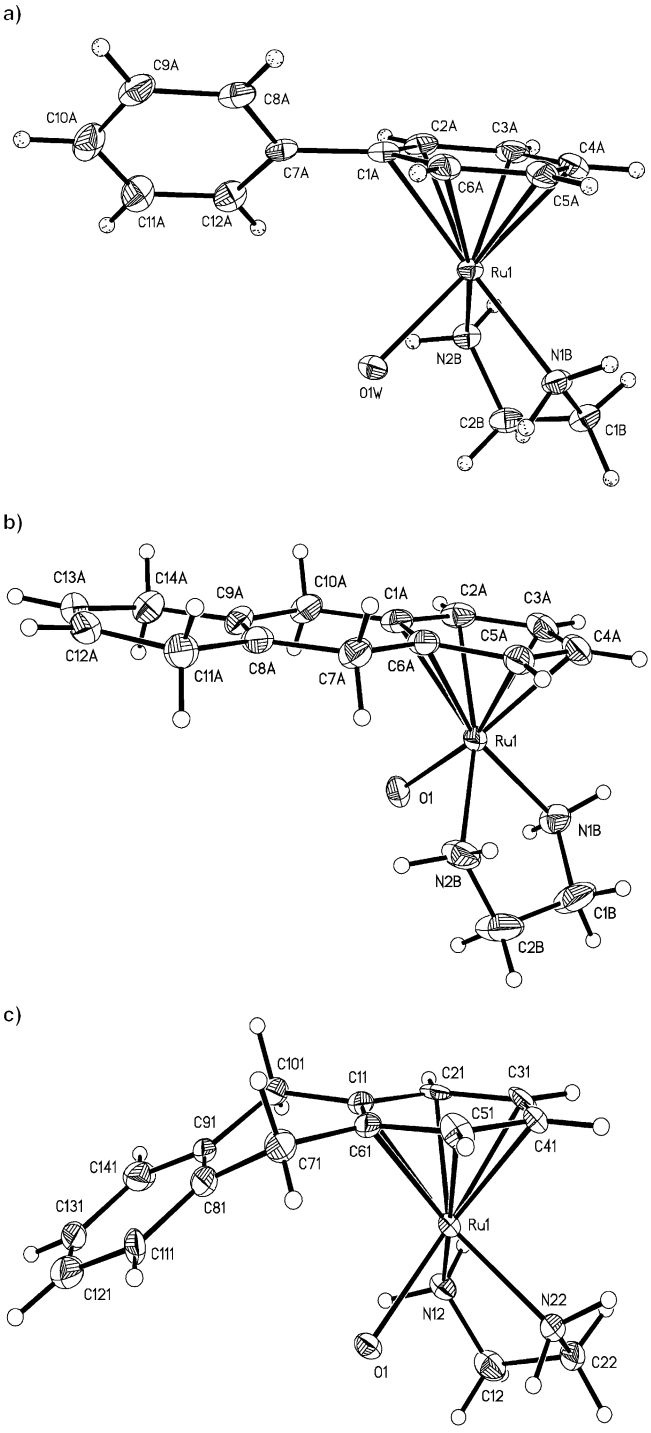

Figure 1. X-ray structures and atom numbering schemes for a) [(η^6-Bip)-Ru(en)$(H_2O)_{0.5}(OH)_{0.5}]^{1.5+}$ in complex **4**, b) [(η^6-THA)Ru(en)$(H_2O)]^{2+}$ in complex **5B**, and c) [(η^6-DHA)Ru(en)$(H_2O)]^{2+}$ (**6a**) in complex **6**, at 30% probability thermal ellipsoids. Complex **5A** and cation **6b** are shown in Figures S1 and S2 in the Supporting Information.

is increased, these peaks shifted to lower frequency as shown for the NH_d protons of complex **4** in Figure 3a. Analysis of the NMR titration curves (Figure 3b) gave pK_a values of 7.71 ± 0.01, 8.01 ± 0.03 and 7.89 ± 0.02 for complexes **4**, **5** and **6**, respectively.

The UV/Vis spectra of the aqua complexes **4**, **5** and **6** all showed significant changes in the region 215–400 nm on

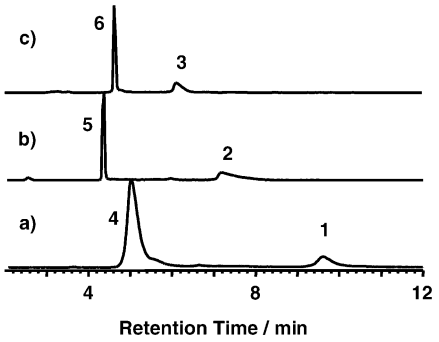

Figure 2. HPLC chromatograms with UV detection at 254 nm for 2 mM equilibrium aqueous solutions of a) [(η^6-Bip)Ru(en)Cl][PF_6] (**1**), b) [(η^6-THA)Ru(en)Cl][PF_6] (**2**), and c) [(η^6-DHA)Ru(en)Cl][PF_6] (**3**). Peak labels: **1**, **2** and **3** correspond to the chloro complex cations, and **4**, **5** and **6** to the corresponding aqua adducts, respectively. Retention times (min) **1**: 9.61, **2**: 7.17, **3**: 6.08, **4**: 5.03, **5**: 4.37, **6**: 4.61.

Table 4. Positive ions detected by HPLC-ESI-MS for aqueous solutions of complexes [(η^6-Bip)Ru(en)Cl][PF_6] (**1**), [(η^6-THA)Ru(en)Cl][PF_6] (**2**) and [(η^6-DHA)Ru(en)Cl][PF_6] (**3**).

	RT [a] [min]	Obs (Calcd)[b] m/z	Observed ions
1	5.03	314.8 (315.0)	$[\mathbf{4}^{2+}$[c]$-H_2O-H$[d]$]^+$
		428.9 (429.0)	$[\mathbf{4}^{2+}-H_2O+TFA]^+$
	9.61	350.9 (351.0)	$\mathbf{1}^+$
2	4.37	343.1 (343.1)	$[\mathbf{5}^{2+}$[c]$-H_2O-H]^+$
		457.1 (457.1)	$[\mathbf{5}^{2+}-H_2O + TFA]^+$
	7.17	379.1 (379.1)	$\mathbf{2}^+$
3	4.61	341.1 (341.1)	$[\mathbf{6}^{2+}$[c]$-H_2O-H]^+$
		455.1 (455.1)	$[\mathbf{6}^{2+}-H_2O+TFA]^+$
	6.08	377.1 (377.0)	$\mathbf{3}^+$

[a] RT is the retention time in HPLC traces (Figure 2). [b] Observed (Obs) and calculated (Calcd) mass-to-charge ratios for the observed ions. Mass type: monoiso. For mass spectra see Figure S3. [c] Complexes **4**, **5** and **6** are the respective aqua adducts of **1**, **2** and **3**. [d] H indicates gain or loss of a proton.

varying the pH from 1 to 11 (for **4**, see Figure 4a), accompanied by two isosbestic points suggesting that the spectral changes arise from an equilibrium involving the aqua and hydroxo complexes. No evidence was found for time-dependent changes on variation of the pH (which might have been indicative of the formation of hydroxo bridged species). This interpretation agrees with the NMR data. The UV/Vis pH titration curve for complex **4** was fitted to the Henderson–Hasselbalch equation giving a pK_a value of 7.71 ± 0.01 from 270 nm data, 7.70 ± 0.04 from 242 nm data (Figure 4b), in agreement with the pK_a value obtained by NMR spectroscopy.

Kinetics of aquation and anation: The time dependences of the absorption spectra of aqueous solutions of complexes **1–3** in 0.1 M $NaClO_4$ at 298 K are shown in Figure 5 (difference spectra) and Figure S4 in the Supporting Information. In each case the presence of an isosbestic point (292, 261 and 259 nm for **1**, **2** and **3**, respectively) suggested a single step reaction, conversion of the initial chloro complexes to the aqua products. The pK_a values of complexes **4**, **5** and **6** are all >7.7 so that the deprotonation of the aqua products is negligible at the pH range of the kinetic studies. The maxi-

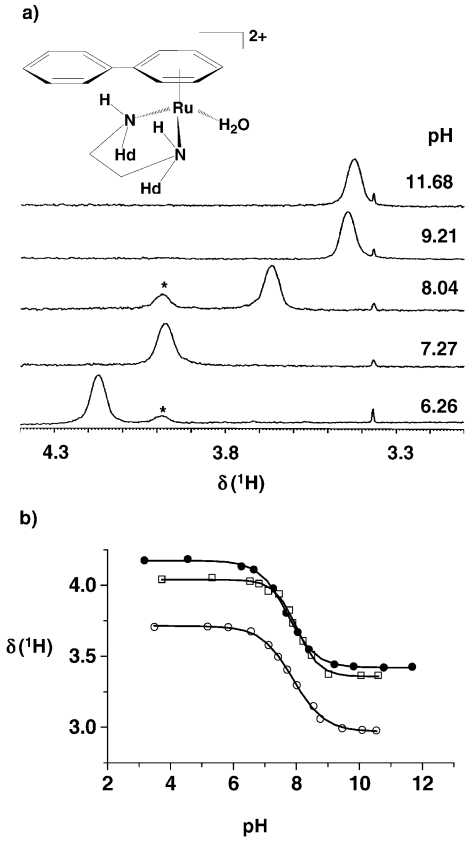

Figure 3. a) Variation of the ^{1}H NMR chemical shift of the NHd protons of $[(\eta^6\text{-Bip})Ru(en)(H_2O)][PF_6]_2$ (**4**, 6 mM) in 100 mM $NaClO_4$, 298 K with pH. The peak labelled * is from residual $[(\eta^6\text{-Bip})Ru(en)Cl][PF_6]$ (**1**). b) Comparison of complexes **4** (●), **5** (□) and **6** (○). The full lines represent computational fits giving the pK_a values listed in Table 5.

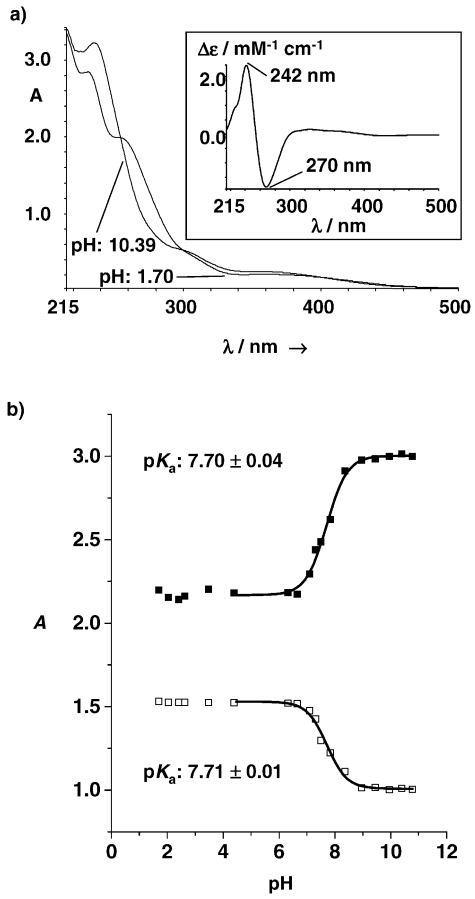

Figure 4. a) UV/Vis spectra for a 0.3 mM aqueous solution of $[(\eta^6\text{-Bip})Ru(en)(H_2O)][PF_6]_2$ (**4**) at pH 1.70 and 10.39, 298 K. The insert shows the difference spectrum. b) Variation of the absorbance at 242 nm (■) and 270 nm (□) with pH. The full lines are computational fits giving the pK_a values shown.

mum change in absorption in the region of 250–500 nm occurred at 319, 316 and 315 nm for **1**, **2** and **3**, respectively. These wavelengths were selected for the subsequent kinetic studies, and the extinction coefficients of the chloro and respective aqua complexes at these wavelengths are listed in Table 5.

The aquation of complexes **1**, **2** and **3** at 298 K in aqueous solutions with various ionic strengths (0.015–0.5 M $NaClO_4$) was monitored at the selected wavelengths as shown in Figure 6 and Figure S5 in the Supporting Information. In each case the time dependence of the absorbance followed first-order kinetics, corresponding to the rate constants k_{H_2O} listed in Table 6. For all three complexes, it can be seen that the rate of aquation was almost independent of ionic strength, and was about twofold faster for the THA and DHA complexes **2** and **3** than for the Bip complex **1**.

The reverse anation reactions were studied by adding excess NaCl to equilibrium solutions of the chloro complexes **1**, **2** and **3**. The anation reactions were rapid (Figure 6 and Figure S5), reaching equilibrium within periods of 100–1600 s. The second-order rate constants k_{Cl} were calculated from the slopes of the plots of the pseudo-first-order rate constants k'_{Cl} vs. $[Cl^-]$ (inserts in Figure 6 and Figure S5) and are listed in Table 6. It can be seen that the anation reactions of the THA and DHA complexes **5** and **6** are about

Table 5. Extinction coefficients (ε) at selected wavelengths (λ) for ruthenium arene complexes, and pK_a values of aqua complexes in 0.1 M $NaClO_4$ at 298 K.

Complex[a]	ε [M^{-1} cm^{-1}](λ [nm])	pK_a
$[(\eta^6\text{-Bip})Ru(en)Cl]^+$ (**1**)	1576 (319)	
$[(\eta^6\text{-THA})Ru(en)Cl]^+$ (**2**)	850.6 (316)	
$[(\eta^6\text{-DHA})Ru(en)Cl]^+$ (**3**)	1090 (315)	
$[(\eta^6\text{-Bip})Ru(en)(H_2O)]^{2+}$ (**4**)	1139 (319)	7.71 ± 0.01
$[(\eta^6\text{-THA})Ru(en)(H_2O)]^{2+}$ (**5**)	590.1 (316)	8.01 ± 0.03
$[(\eta^6\text{-DHA})Ru(en)(H_2O)]^{2+}$ (**6**)	775.0 (315)	7.89 ± 0.02

[a] pH values all within range of 6.29–6.41 (aqua complexes).

2.5-fold faster than that of the biphenyl complex **4**, and that the rates decrease by about twofold on increasing the ionic strength from 0.015 to 0.5 M ($NaClO_4$).

The rates of the aquation and anation reactions in 100 mM $NaClO_4$ were also determined at 288 and 310 K (Table 6, Figures S6–S8 in the Supporting Information) which allowed the Arrhenius activation energy (E_a), activation enthalpy ($\Delta H^{\neq}$) and activation entropy ($\Delta S^{\neq}$) to be determined (Figure S9; see Supporting Information). The activation parameters resulting from the Arrhenius and Eyring plots for the aquation and anation of complexes **1**/**4** are listed in Table 7, and for **2**/**5** and **3**/**6** in Table S3. The reactions of complexes **2**/**5** and **3**/**6** were faster than those of **1**/**4**,

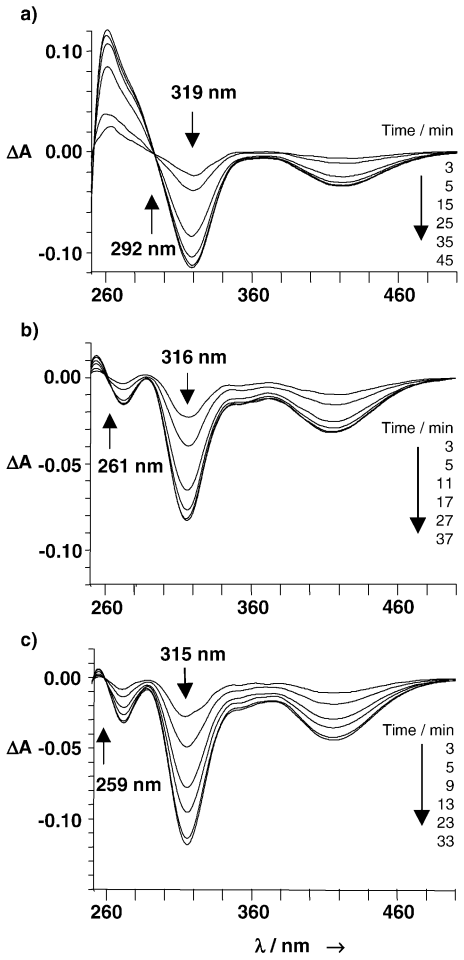

Figure 5. Time evolution of UV-Vis difference spectra for the aquation of a) $[(\eta^6\text{-Bip})Ru(en)Cl][PF_6]$ (**1**) (0.3 mM, pH 6.29), b) $[(\eta^6\text{-THA})Ru(en)Cl][PF_6]$ (**2**) (0.5 mM, pH 6.37), and c) $[(\eta^6\text{-DHA})Ru(en)Cl][PF_6]$ (**3**) (0.5 mM, pH 6.41) in 100 mM $NaClO_4$ solution at 298 K. The down arrows indicate the wavelengths selected for subsequent kinetic studies, and the up arrows indicate isosbestic points. $\Delta A = A_t - A_0$, where A_t = absorbance at time t, and A_0 = absorbance at $t = 0.5$ min (i.e. immediately after dilution of methanol solutions with water).

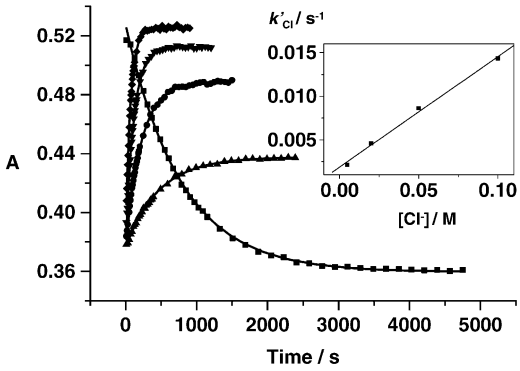

Figure 6. Time-dependence of the absorbance at 319 nm for the hydrolysis of 0.3 mM $[(\eta^6\text{-Bip})Ru(en)Cl][PF_6]$ (**1**) in 100 mM $NaClO_4$ solution at 298 K. The full lines represent computer fits giving the first order rate constants listed in Table 6 for aquation, and pseudo-first order rate constants for anations. Labels: aquation (■), anation with addition of 5 (▲), 20 (●), 50 (▼) or 100 (◆) mM NaCl to the hydrolysis equilibrium solution.

Table 7. Activation parameters for the aquation of complex **1** and the anation of complex **4**.

Complex	E_a [kJ mol^{-1}]	$\Delta H^{\neq}$ [kJ mol^{-1}]	$\Delta S^{\neq}$ [J K^{-1} mol^{-1}]
$[(\eta^6\text{-Bip})Ru(en)Cl]^+$ **1**	75.6 ± 0.6	73.1 ± 0.6	−55.7 ± 2.0
$[(\eta^6\text{-Bip})Ru(en)(H_2O)]^{2+}$ **4**	76.7 ± 1.3	74.1 ± 1.3	−13.6 ± 4.5

so the errors of the measurements over the accessible temperature range are higher. To assess further the reliability of the activation parameters, the variation with temperature of the aquation rate constant for the benzene complex **7**, $[(\eta^6\text{-benzene})Ru(en)Cl][PF_6]$, was also determined by the same method (Table S3 and Figure S10 in the Supporting Information). It can be seen that $\Delta S^{\neq}$ values are negative for the aquation or anation reactions of all seven complexes (except aquation of complex **3**).

Table 6. Rate and equilibrium constants for aquation of complexes **1–3** at various ionic strengths and temperatures.

$[NaClO_4]$ [M^{-1}]	T [K]	k_{H_2O} [10^{-3} s^{-1}]	$(t_{1/2})_{H_2O}$ [min]	k_{Cl} [M^{-1} s^{-1}]	K [10^{-3} M]
		$[(\eta^6\text{-Bip})Ru(en)Cl][PF_6]$[a] **1**			
0.015	298	1.28 ± 0.01	9.02 ± 0.04	0.146 ± 0.009	8.8 ± 0.6
0.1	288	0.42 ± 0.02	27.5 ± 1.4	0.045 ± 0.001	9.3 ± 0.7
0.1	298	1.23 ± 0.01	9.39 ± 0.03	0.127 ± 0.006	9.7 ± 0.5
0.1	310	3.95 ± 0.09	2.92 ± 0.07	0.435 ± 0.029	9.1 ± 0.9
0.25	298	1.23 ± 0.01	9.39 ± 0.06	0.096 ± 0.008	12.8 ± 1.1
0.5	298	1.28 ± 0.01	9.02 ± 0.07	0.088 ± 0.005	14.5 ± 0.9
		$[(\eta^6\text{-THA})Ru(en)Cl][PF_6]$[a] **2**			
0.015	298	2.36 ± 0.02	4.90 ± 0.04	0.360 ± 0.014	6.6 ± 0.3
0.1	288	0.60 ± 0.01	19.2 ± 0.3	0.091 ± 0.017	6.6 ± 1.6
0.1	298	2.26 ± 0.01	5.11 ± 0.02	0.306 ± 0.022	7.4 ± 0.6
0.1	310	6.84 ± 0.07	1.69 ± 0.02	0.583 ± 0.028	11.7 ± 0.7
0.5	298	2.59 ± 0.02	4.26 ± 0.06	0.169 ± 0.011	15.3 ± 1.2
		$[(\eta^6\text{-DHA})Ru(en)Cl][PF_6]$[a] **3**			
0.015	298	2.23 ± 0.02	5.18 ± 0.05	0.347 ± 0.019	6.4 ± 0.4
0.1	288	0.40 ± 0.03	28.9 ± 1.5	0.072 ± 0.004	5.6 ± 0.6
0.1	298	2.15 ± 0.03	5.37 ± 0.08	0.293 ± 0.018	7.3 ± 0.6
0.1	310	6.49 ± 0.10	1.78 ± 0.03	0.722 ± 0.020	9.0 ± 0.4
0.5	298	2.44 ± 0.02	4.73 ± 0.04	0.144 ± 0.010	16.9 ± 1.4

[a] Initial concentration: 0.3 mM for **1**, 0.5 mM for **2** and **3**, and pH: **1** 6.29, **2** 6.37, **3** 6.41.

The values of the equilibrium constants for all hydrolysis reactions were calculated from the ratios of k_{H_2O}/k_{Cl} and are listed in Table 6. The constants increase with ionic strength and are similar for all three complexes. In the presence of 0.1 M $NaClO_4$, about 8.8% of complex **1** is aquated in an equilibrium aqueous solution containing 100 mM NaCl at 298 K. For complexes **2** and **3**, under the same conditions the proportions are 6.9% and 6.8%, respectively.

The equilibrium constants (K_{an}) for the anation reactions of aqua complexes **4–6** in 100 mM $NaClO_4$ at 298 K were also determined by spectropho-

tometric titration as 109.1, 129.6 and 133.9 M^{-1}, respectively. These values give equilibrium constants K_{aq} ($K_{aq}=1/K_{an}$) for the respective aquation reactions of 9.2×10^{-3}, 7.7×10^{-3} and 7.5×10^{-3} M, respectively, in agreement with the values obtained from kinetic data (Table 6).

Discussion

The aqua adducts of the anticancer complexes [(η^6-arene)-Ru^{II}(en)Cl]$^+$ may play key roles in the biological mechanism of action of this class of complexes. We studied the aquation and anation rates, and characterised the aqua complexes by HPLC, mass spectrometry, NMR spectroscopy and X-ray crystallography. The chloro and hydroxo adducts appear to be less reactive than the aqua adducts,[5] and the pK_a values of the aqua complexes were therefore also determined.

Structures of aqua ruthenium arene complexes: To prepare crystalline aqua complexes, the coordinated chloride ligands were removed from the chloro ruthenium arene complexes **1**–**3** by addition of $AgPF_6$. $AgNO_3$ was avoided because of the possible coordination of the nitrate ligand to Ru, as reported for crystals of α-[$Ru(azpy)_2(NO_3)_2$][8] and *cis*-[$Pt(NH_3)_2(NO_3)_2$].[9]

The X-ray structures of **4**–**6** revealed coordinated Ru–$O(H_2)$ bond lengths of 2.1–2.2 Å (Table 2 and Table S2 in the Supporting Information), within the range reported for other aqua Ru arene compounds.[10] The coordinated OH_2 ligand showed acidity through deprotonation as revealed in solid state structures of **4** and **5A**, where about 50% of the aqua ligands in the unit cell are deprotonated in each case. There is an interesting arene conformation for each aqua compound as shown in Figure 1 and Table 3. Notably, the propeller twist of the biphenyl in **4** is 19.1° larger than that in chloro complex **1**. For the aqua THA complex **5**, the small hinge bending of 11.6° down toward the O atom in cation **5A** and of 1.8° away from the O atom in cation **5B** shows that the tricyclic ring system is still rather flat as in the chloro THA complex **2**. For the aqua DHA complex **6**, the outer ring (C) is significantly bent down toward the O atom by 31.8° (**6a**, 38.4°(**6b**)), comparable with the hinge bending of 40.6° in the chloro complex **3**. Such large hinge bending toward the O atom in the DHA complex **6** may impose a steric constraint G N7 coordination in reactions with DNA. For the biphenyl complexes **1** and **4**, the propeller twist of the biphenyl ring may present an even larger steric constraint towards aquation and DNA binding.

Effects of ionic strength and temperature on hydrolysis rates: The rate constants for aquation of the chloro complexes **1**–**3** are almost independent of the ionic strength, but the rate constants for anation of the aqua complexes **4**–**6** all decrease with increase in the ionic strength (Table 6). This result is in agreement with the prediction of the Brønsted equation:[11] the rate constant is expected to be independent of the ionic strength when one of the reactants is uncharged, whereas the rate constant decreases with ionic strength if the charges on the two ions are of opposite sign.

When the temperature was increased from 288 to 310 K, the rate constants for hydrolysis of complexes **1**, **2** and **3** in 0.1 M $NaClO_4$ increased by about 9-, 11- and 16-fold, respectively, while the rate constants for anation of the aqua complexes **4**, **5** and **6** in 0.1 M $NaClO_4$ at 310 K were about 10-, 6- and 10-fold, respectively, higher than those at 288 K. The activation parameters resulting from the Arrhenius and Eyring plots for the aquation and anation of complexes **1**–**6** (Table 7 and Table S3) show that the mean $\Delta S^{\neq}$ values for both reactions are negative, except for the aquation of complex **3**. Unfortunately, the activation parameters, especially the activation entropies for complexes **2**/**5** and **3**/**6** are subject to large errors. The rate constant for aquation of the benzene analogue **7**, 1.98×10^{-3} s^{-1} at 298 K, is intermediate between that of complexes **1** and **2**, and the errors associated with the activation parameters are also between those for complexes **1** and **2** (Table S3 in the Supporting Information). This indicates that the lower errors for the activation parameters of complexes **1**/**4** and **7** are reliable, and that the higher errors for complexes **2**/**5** and **3**/**6** result not only from the small accessible temperature range but also from the fast rate of the reactions. The apparent negative entropies for the reactions of complexes **1**/**4** and **7** suggest that hydrolysis of this class of ruthenium(II) arene complexes occurs by an associative pathway (vide infra).

Relationship between structure, aquation and anation rates: The pseudo-first-order rate constants for the anation of the aqua arene complexes **4**–**6** are within the range of 1.3–3.1 × 10^{-2} s^{-1} (Table S2; see the Supporting Information). These are comparable with the rate constants for water exchange on $[Ru(H_2O)_6]^{2+}$[12] (1.8×10^{-2} s^{-1}), but 100× lower than that (11.5 s^{-1}) for [(η^6-C_6H_6)$Ru(H_2O)_3$]$^{2+}$.[13] Although there is a strong *trans*-labilising effect of the benzene ligand in [(η^6-C_6H_6)$Ru(H_2O)_3$]$^{2+}$,[13] this was not observed for anation of the ethylenediamine ruthenium(II) arene complexes **4**–**6**. This implies that, in the current work, the chelate ligand en slows down the anation rate. For complexes **1**–**3** [(η^6-arene)-Ru(en)Cl]$^+$ (arene = biphenyl (Bip), 5,8,9,10-tetrahydroanthracene (THA), 9,10-dihydroanthracene (DHA)), the rate constants ($1.23–2.26\times10^{-3}$ s^{-1}) are much lower than that for *cis*-[$Ru(H_2O)_4Cl_2$][14] (130×10^{-3} s^{-1}; see Table S2 in the Supporting Information), also indicating that the en ligand in [(η^6-arene)Ru(en)Cl]$^+$ reduces the lability of the leaving group Cl^-.

The effect of chelate ligands on substitution reactions is dependent on the nature of the central metal and the position of the chelate ligand relative to the leaving group. Chelate ligands such as en in *cis*- and *trans*-[$Co(en)_2Cl_2$]$^+$[15] and 2,2′-bipyridine (bpy) in [(η^6-C_6H_6)Ru(bpy)(H_2O)]$^{2+}$[16] slow down the substitution of the labile groups chloride and water. In contrast, for the ruthenium(III) complexes[17] [$Ru(NH_3)_5Cl$]$^{2+}$, *cis*-[$Ru(NH_3)_4Cl_2$]$^+$, *cis*-[$Ru(en)_2Cl_2$]$^+$, *cis*-[$Ru(en)_2(H_2O)Cl$]$^{2+}$, *cis*-α-[$Ru(trien)Cl_2$]$^+$ and cobalt(III) complex β-[$Co(trien)Cl_2$]$^+$,[18] the hydrolysis rate increases with increase in chelation. The present work indicates that for (η^6-arene)ruthenium(II)en complexes, the en ligand *cis* to

the leaving group Cl^- or H_2O, as for the bpy ligand in $[(\eta^6\text{-}C_6H_6)Ru(bpy)(H_2O)]^{2+}$, slows down the aquation and anation reactions due to its electronic and steric effects.

Reaction mechanism: The X-ray structures[1,19] show that the Ru–Cl bond lengths in complexes **1–3** (2.408(15), 2.405(6) and 2.407(9) Å, respectively) are almost the same. However, the hydrolysis rates of the THA and DHA complexes **2** and **3** are about 2× faster than that of the Bip complex **1**, implying that bond-breaking alone is not rate-controlling in this case and suggesting that an associative interchange mechanism (I_a) applies to the substitution reactions of the ruthenium(II) arene complexes studied here. The negative $\Delta S^{\neq}$ values (Table 7) support this conclusion. It might be expected that I_a substitution reactions would be more influenced by steric factors than those which occur by I_d pathways. Indeed, the aquation and anation of the Bip complexes **1** and **4** are slowed down by the steric hindrance of the pendant phenyl ring twisting towards the labile groups Cl^- and H_2O. Crowding around the central atom does not favour the formation of associative states with a higher coordination number (seven).[15] Additional support for an I_a mechanism is provided by studies on the kinetics of reactions with other nucleophiles.[20] The rates of aquation of the complexes $[(\eta^6\text{-biphenyl})Ru(en)X]^+$ X = Cl, Br and I follow the order Cl ~ Br > I, consistent with an associative mechanism in which bond-making and not bond-breaking is rate-controlling.

The acidic hydrolysis of ruthenium(III) complexes such as $[Ru(NH_3)_4X_2]^+$, $[Ru(NH_3)_5X]^{2+}$ ($X = Cl^-$, Br^-, I^-) occurs by an S_N2 associative pathway.[17a] Bond making is more important than bond breaking. The strong dependence of the substitution rate on the nature of incoming group in substitution reactions of $[Ru(EDTA)(H_2O)]^-$,[21] and the complete stereoretention in the substitution and hydrolysis reactions of chiral ruthenium(III) complexes[22] also support predominant associative pathways. In contrast, most ruthenium(II) complexes tend to react *via* dissociative pathways.[12] The rates of substitution of the pyridine (py) ligand in ruthenium(II) complexes such as *cis*-$[Ru(phen)_2(py)_2]^{2+}$ by X^- (Cl^-, Br^-, I^-, NCS^-, N_3^-, NO_2^-) are independent of the nature of X[23] and these complexes are thought to react by I_d pathways.

However, π-acid ligands such as benzene in $[(\eta^6\text{-}C_6H_6)Ru(H_2O)_3]^{2+}$ are thought to accept electron density from the central ruthenium atom to produce a higher charge on the metal. Thus Ru^{II} in $\{(\eta^6\text{-}C_6H_6)Ru^{II}\}^{2+}$ behaves like a Ru^{III} centre.[13] This electronic effect makes the substitution reactions of the ruthenium(II) complexes $[(\eta^6\text{-}C_6H_6)Ru(H_2O)_3]^{2+}$ appear to occur by interchange pathways in which bond-breaking is only slightly less favourable than bond-making. A similar effect has been reported for water substitution reactions of the complexes $[(\eta^6\text{-X})Ru(bpy)(H_2O)]^{2+}$ (X = benzene, *p*-cymene or hexamethylbenzene), though the rates were said to be only slightly affected by the nature of the entering ligand L (L = H_2O, SCN^-, I^-, Br^-, N_3^-).[16] Therefore, strong π-acid ligands such as Bip, THA and DHA might be responsible for the shift towards a more associative pathway in the $I_d \leftrightarrow I_a$ mechanistic continuum for the (η^6-arene)ruthenium(II)(en) complexes studied here.

Speciation of ruthenium complexes in plasma and cell nucleus: We can use the pK_a values of (η^6-arene)Ru^{II}(en) aqua adducts and equilibrium constants for aquation of the chloro complexes in Table 5 and Table 6 to predict the speciation of these chloro anticancer complexes under various biological conditions (Table 8).

Table 8. Speciation of ruthenium arene anticancer complexes in blood plasma, the cell cytoplasm and nucleus, pH 7.4, 310 K.

Complex	[Ru][a] [μM]		[Cl^-] [mM]	% species X = Cl	H_2O	OH
$[(\eta^6\text{-Bip})Ru(en)X]^{n+}$	5.0	plasma	104	92.0	5.2	2.8
	5.0	cytoplasm	22.7	71.4	18.6	10.0
	5.0	nucleus	4	30.5	45.2	24.3
$[(\eta^6\text{-THA})Ru(en)X]^{n+}$	0.5	plasma	104	89.9	8.8	1.3
	0.5	cytoplasm	22.7	66.0	29.7	4.3
	0.5	nucleus	4	25.4	65.2	9.4
$[(\eta^6\text{-DHA})Ru(en)X]^{n+}$	2.0	plasma	104	92.1	5.6	2.3
	2.0	cytoplasm	22.7	71.6	20.2	8.2
	2.0	nucleus	4	30.8	49.1	20.1

[a] Initial concentration of chloro complexes are the IC_{50} values.[2]

In blood plasma, the Cl^- concentration is high, about 104 mM, and all three complexes would exist largely (> 89%) in their chloro forms. In contrast, the chloride concentrations in the cell cytoplasm and cell nucleus are much lower, about 22.7 and 4 mM, respectively.[24] Hence the extent of aquation would increase from about 30% in the cytoplasm to about 70% in the nucleus. This would represent an activation mechanism for these chloro (η^6-arene)-Ru^{II}(en) complexes since the Ru–Cl adducts react much more slowly with nucleotides such as 5′-GMP than the Ru–OH_2 adducts and aquation is the initial step in reactions of the chloro complexes.[5]

Only small amounts (< 10% of the total Ru^{II} arene complexes) of hydroxo adducts are predicted to exist inside cells since the pK_a values of the aqua complexes are all relatively high (7.7–8.0). We found previously that arene Ru^{II} aqua complexes reacted with guanine nucleotides much more slowly at pH 9 compared to pH 7.[5] At pH 9 they would exist largely as Ru–OH complexes and, just as with Pt^{II} diam(m)ine complexes it seems that Ru–OH bonds are less reactive than Ru–OH_2 bonds.

For cisplatin, the hydrolysis products are present mostly as hydroxo forms both in plasma and in the cell nucleus due to the higher acidity of the aqua adducts (pK_a *cis*-$[Pt(NH_3)_2Cl(H_2O)]^+$ 6.41, *cis*-$[Pt(NH_3)_2(H_2O)_2]^{2+}$ 5.39 and 7.21),[25] although the extent of aquation is higher than that for the ruthenium(II) arene complexes. In the cell nucleus, the chloride concentration is about 4 mM, and the dominant species for cisplatin are unreactive hydroxo forms, including the monohydroxo species *cis*-$[PtCl(OH)(NH_3)_2]$ (30%) and dihydroxo species *cis*-$[Pt(OH)_2(NH_3)_2]$ (35%).[24b]

Conclusion

The aquation reactions of en Ru^{II} arene complexes **1–3** reach equilibrium within 50 min at 298 K. This is an order of

magnitude faster than platinum diam(m)ine complexes such as cisplatin. The twofold difference in rate between the biphenyl complex **1** and the tetrahydroanthracene complex **2** or the dihydroanthracene complex **3** suggests that variations in the steric and electronic effects of arene ligands modulate the aquation rate. Since the anation reactions are rapid, the equilibrium constants for hydrolysis are small ($K = 7.3–9.7 \times 10^{-3}$ M, 298 K, $I = 0.1$ M ($NaClO_4$)). Hence in blood plasma these complexes will exist largely as the less reactive chloro complexes and the percentage of aqua species will increase markedly in the cell cytoplasm and nucleus where the chloride concentrations are lower (22.7 and 4 mM, respectively).

Variation of the arene had little effect on the pK_a of the coordinated water ligands. Since the pK_a values were high (7.7–8.0), only small amounts of the less reactive hydroxo species would be present at biological pH (7.2–7.4). However hydroxo adducts of complexes **4** and **5** readily co-crystallised with the aqua adducts even at pH 3–6. Whereas the tetrahydroanthracene ligand remains relatively flat in the aqua complexes, as it is in the chloro complex, the dihydroanthracene ligand is significantly bent towards the coordinated oxygen. The biphenyl ligand in the aqua complex **4** has a relatively large propeller twist. These structural features illustrate how the arene ligand can influence access to the substitution site. The variation of rate constants of complexes **1**, **2** and **3** indicates that bond-breaking is not rate-controlling and suggests that the hydrolysis reactions of the chloro (arene)Ru^{II}en complexes occur by associative pathways. The electronic effect of arene ligands may account for the shift from an I_d towards an I_a pathway.

These findings show that there are some common features in the aqueous chemistry of arene Ru^{II} ethylenediamine and Pt^{II} diam(m)ine chloro anticancer complexes. Both undergo hydrolysis in water, which is largely suppressed at blood chloride concentration. Such hydrolysis can be the rate-limiting step for interaction of these complexes with DNA bases. It should be possible to control both the rate and extent of hydrolysis of organometallic Ru^{II} complexes with variation in the arene, the monodentate (halide and other) ligand, and the chelate ligand (en), and such changes may aid the optimisation of the anticancer activity of this class of complexes.

Experimental Section

Chemicals: NaCl and $NaClO_4$ were purchased from Fisher Chemicals, $AgNO_3$, $AgPF_6$ and ruthenium atomic absorption standard solution (1030 μg mL^{-1} in 5 wt% HCl) from Aldrich, and CF_3COOH (TFAH) from Arcos.

Preparation of chloro ruthenium complexes: [(η^6-Bip)Ru(en)Cl][PF_6] (**1**), [(η^6-THA)Ru(en)Cl][PF_6] (**2**), [(η^6-DHA)Ru(en)Cl][PF_6] (**3**) and [(η^6-benzene)Ru(en)Cl][PF_6] (**7**) were synthesised as described previously.[1,19]

Preparation of crystalline of aqua ruthenium complexes: A solution of $AgPF_6$ (1.3 mol equiv) in H_2O was added to a solution of [(η^6-arene)-Ru(en)Cl][PF_6] (complex **1**: 100 mg, 0.20 mmol; complex **2**: 49.4 mg, 0.09 mmol; or complex **3**: 61 mg, 0.12 mmol) in H_2O (20 mL), giving a yellow-orange solution and an immediate precipitate of AgCl. This mixture was stirred overnight at 313 K (protected from light) and was then filtered to remove AgCl. Evaporation of the solution to dryness gave a dark-yellow product. This was recrystallised from water to afford a crop of fine yellow crystals, which were then recrystallised a second time from water at 277 K to give yellow needles suitable for X-ray structure determination.

[(η^6-Bip)Ru(en)(H_2O)][PF_6]$_2$ (**4**): ^{1}H NMR (10% D_2O/90% H_2O, 500 MHz, 298 K,): $\delta = 7.800$ (m, 2H), 7.618 (m, 3H), 6.116 (d, 2H), 5.991 (t, 2H), 5.844 (t, 1H), 5.967 (broad, 2H), 3.768 (broad, 2H), 2.455 (m, 2H), 2.390 ppm (m, 2H).

[(η^6-THA)Ru(en)(H_2O)][PF_6]$_2$ (**5**): ^{1}H NMR (10% D_2O/90% H_2O, 500 MHz, 298 K): $\delta = 6.057$ (broad, 2H), 5.863 (s, 2H), 5.808 (m, 2H), 5.729 (m, 2H), 4.045 (broad, 2H), 3.357 (q, 2H), 3.015 (q, 2H), 2.760 (s, 4H), 2.448 (m, 2H), 2.368 ppm (m. 2H).

[(η^6-DHA)Ru(en)(H_2O)][PF_6]$_2$ (**6**): ^{1}H NMR (10% D_2O/90% H_2O, 500 MHz, 298 K): $\delta = 7.473$ (m, 2H), 7.407 (m, 2H), 5.954 (m, 2H), 5.857 (m, 2H), 5.737 (broad, 2H), 3.98 (q, 2H), 3.864 (q, 2H), 3.654 (broad, 2H), 2.10 (m, 2H), 2.011 ppm (m, 2H).

Preparation of NMR and UV/Vis samples: For solution work, stock solutions of the aqua complexes **4**, **5** and **6** were prepared as follows: aliquots of the chloro complexes **1**, **2** or **3** were dissolved in methanol (1 mL) and the Ru concentration (5–10 mM) was determined by ICP-AES. Then one mol equiv of $AgNO_3$ (an aliquot of a 100 or 50 mM aqueous solution) was added and left to react for 24 h in the dark. The precipitate of AgCl was removed by filtration and the resulting aqua complexes were used for the determination of pK_a values by UV/Vis spectroscopy. For 1D ^{1}H NMR experiments aliquots of the solutions were lyophilised and re-dissolved in 10% D_2O/90% H_2O containing 0.1 M $NaClO_4$.

Ultraviolet and visible (UV/Vis) spectrometry: A Perkin-Elmer Lambda-16 UV/Vis recording spectrophotometer was used with 1 cm path-length quartz cuvettes (0.5 mL) and a PTP1 Peltier temperature controller. Spectra were processed using UVWinlab software for Windows′ 95.

High-performance liquid chromatography–electrospray ionisation mass spectrometry (HPLC-ESI-MS): Positive-ion electrospray ionisation mass spectra were obtained with a Platform II mass spectrometer (Micromass, Manchester, U.K.). A Waters 2690 HPLC system was interfaced with the mass spectrometer, using a PLRP-S reversed-phase column (250 × 4.6 mm, 100 Å, 5 μm, Polymer Labs). Mobile phase: 25% acetonitrile (for HPLC application, Fisher Chemicals)/75% water (purified using a Millipore Elix 5 system) containing 0.1% (for complex **1**) or 0.01% (for complexes **2** and **3**) TFA as the ion-pairing reagent with a flow rate of 1.0 mL min^{-1} and a splitting ratio of 1/6. The spray voltage and the cone voltage were 3.50 kV and 20 V, respectively. The capillary temperature was 373 K with a 450 L h^{-1} flow of nitrogen drying gas. The quadrupole analyser, operated at a background pressure of 2×10^{-5} Torr, was scanned at 900 Da s^{-1}. Data were collected and analysed on a Mass Lynx (ver. 2.3) Windows NT PC data system using the Max Ent Electrospray software algorithm and calibrated versus an NaI calibration file.

NMR spectroscopy: 1D ^{1}H NMR spectra were acquired at a temperature of 298 K on a Bruker DMX500 NMR spectrometer equipped with a triple resonance (^{1}H, ^{13}C, ^{15}N) *z*-gradient probehead, using 32 transients into 32 k data points over a frequency width of 7 kHz and using presaturation to suppress the water resonance. All NMR data were processed using Xwin-nmr (Version 2.0, Bruker U.K. Ltd.).

Inductively coupled plasma atomic emission spectrometry (ICP-AES): Stock solutions of ruthenium complexes **1**–**3** (5–10 mM) in methanol were diluted with deionised water for Ru determination using an IRIS plasma spectrometer (Thermo Jarrell Ash Co.) with ThermoSPEC/CID software.

pH measurements: All pH measurements were made using a Corning 240 pH meter equipped with an Aldrich micro combination electrode calibrated with Aldrich standard buffer solutions of pH 4, 7 and 10. For NMR samples in 10% D_2O/90% H_2O, no correction has been applied for the effect of deuterium on the glass electrode.

pH titrations: a) NMR samples. NMR samples of aqua complexes **4** and **5** (5 mM), **6** (3 mM) were prepared in 10% D_2O/90% H_2O, and the values of pH were adjusted with 0.01–1 M NaOH or $HClO_4$ as appropriate. A small amount of leakage of Cl^- ions from the combination electrode into the NMR solutions occurred (reduction in intensity of peak for aqua complex, appearance of new peak for chloro complex) but this did not affect the shifts of the aqua/hydroxo species. b) UV/Vis samples. For the UV/Vis titration, an aliquot (13.2 μL) of a stock solution of the aqua complex **4** (9.09 mM) was diluted to 400 μL with 100 mM $NaClO_4$ solution to which 0.01–1 M NaOH or $HClO_4$ was added to give a range of pH

values. Immediately after recording the absorption spectrum, the pH value was determined using a glass electrode.

X-ray crystallography: Single crystal diffraction data were collected with $Mo_{K\alpha}$ radiation on a Bruker SMART APEX CCD diffractometer equipped with an Oxford Cryosystems low temperature device operating at 150 K. Absorption corrections were applied by using the SADABS[26] procedure (based on an algorithm given by Blessing[27]). The structures of **4**, **5A** and **6** were solved by Patterson methods (DIRDIF),[28] the structure of **5B** was solved by direct methods (SHELXTL).[29] Data collection and refinement parameters are listed in Table 1. All four of the structures exhibit either disorder or twinning. Data analyses utilised the program PLATON.[30]

The two independent PF_6^- ions in **4** are both disordered over two orientations; in one case the disorder components are related by a crystallographic twofold axis. Similarity restraints were applied to chemically equivalent PF distances and FPF angles. The ratio of Ru to PF_6^- in the unit cell of **4** is 8:12, suggesting that the oxygen atom attached to Ru can be assigned to a 1:1 mixture of OH_2 and OH. Though it is rare, there are five crystal structures in the Cambridge Database[31] which contain terminal OH attached to Ru^{II}. The average Ru–OH distance in these structures is 1.922(11) Å, with a range of 1.897–1.978 Å. A similar search for terminal Ru^{II}–OH_2 moieties (56 structures) yielded an average Ru–O distance of 2.133(5) Å with a range of 2.058–2.218 Å. Based on these data, a disordered Ru–OH/Ru–OH_2 moiety might be expected to exhibit a Ru–O distance of about 2.02 Å. The Ru1–O1W distance in **4** is 2.090(4) Å and rather long compared with this value, although given the rather wide ranges spanned by the literature bond lengths and the lengths of the only ordered Ru–OH_2 bonds observed in this series (2.161(5) and 2.155(5) Å in **6**), perhaps not unreasonably so. The anisotropic displacement parameter of O1W also seems quite normal, and shows no elongation along the Ru–O vector. There is thus little direct crystallographic evidence for our proposed disorder model, except that other possible explanations for the observed unit cell stoichiometry, such as partial occupancy of the PF_6^- sites or a mixture of Ru oxidation states, seem rather less plausible.

Similar OH/OH_2 disorder is observed in the structure of **5A**, which also contains disordered PF_6^- ions. There is no question of this kind of disorder in the crystal structure of **5B**, though in this case the water molecule is disordered over two positions in response to the positions of a disordered water of crystallisation. The two Ru–O distances were restrained to be equal.

Crystals of **6** were twinned and generally of rather poor quality. The diffraction pattern was indexed by using the program GEMINI,[32] and the twin law, a twofold rotation about **a*** identified with ROTAX.[33] This operation can be expressed by the matrix I and reflections from the two domains of the crystal were considered to be overlapped if they lay within 0.07 $Å^{-1}$. The structure was refined against F using data with $I > 3\sigma(I)$ using the program CRYSTALS.[34] Aqua-hydrogen positions could not be identified in Fourier maps, and were left out of the model, although it is clear from the O···O contact distances in the structure that a hydrogen bonded network is formed.

$$\begin{pmatrix} 1 & 0.057 & 0.131 \\ 0 & -1 & 0 \\ 0 & 0 & -1 \end{pmatrix} \qquad \text{(I)}$$

CCDC-199475 (**5B**), CCDC-199476 (**4**), CCDC-199477 (**6**), and CCDC-199478 (**5A**) contain the supplementary crystallographic data for this paper. These data can be obtained free of charge via www.ccdc.cam.ac.uk/conts/retrieving.html (or from the Cambridge Crystallographic Data Centre, 12 Union Road, Cambridge CB2 1HZ, UK; Fax: (+44) 1223-336033 or deposit@ccdc.cam.ac.uk).

Kinetic analyses: a) For aquation studies, aliquots (12 μL for **1**, 20 μL for **2**, or 40 μL for **3**) of stock solutions of the chloro complexes **1** (10 mM), **2** (10 mM) or **3** (5 mM) in methanol were diluted to 400 μL with 0.015–0.5 M aqueous $NaClO_4$, and the absorbance at selected wavelengths was then recorded at 20 s intervals. The absorbance/time data for each complex were computer-fitted to the first-order rate equation [Eq. (1)], which gave the k_{H2O} value (k) for each aquation, where C_0 and C_1 are computer-fitted constants, A is the absorbance corresponding to time t.

$$A = C_0 + C_1 e^{-kt} \qquad (1)$$

b) For the measurement of rate constants of the anation reactions, solutions containing 0.3 mM **1**, 0.5 mM **2** or **3**, in presence of various concentrations of $NaClO_4$ (0.015–0.5 M) were left to equilibrate overnight. An aliquot (392 or 390 μL) of the hydrolysis equilibrium solution was transferred into the UV cell, and the initial absorbance was recorded at the selected wavelength. Then an aliquot of an NaCl solution (8 μL of 5, 2.5, or 1 M, or 10 μL 0.2 M NaCl) was added to the above solution and the absorbance was determined at 6–20 s intervals to allow measurement of the pseudo-first-order rate constants. Finally, the second-order rate constants k_{Cl} of the anation reactions were calculated from the slope of plots of the pseudo-first-order rate constants (k'_{Cl}) versus chloride concentration [Cl^-]. All kinetic data were computer-fitted to the appropriate equation using the programme Microcal Origin 5.0.

Measurement of equilibrium constants *K*: a) the equilibrium constants K_{aq} for the aquation reactions were calculated from $K_{aq} = k_{H_2O}/k_{Cl}$. b) In order to confirm the precision of the equilibrium constants obtained from the kinetic data, the equilibrium constants K_{an} (=[Ru(Cl)]/[Ru(H_2O)][Cl^-], where [Ru(H_2O)] and [Ru(Cl)] represent the concentration of aqua and chloro complexes, respectively) for the anation reactions of complexes **4**–**6** in 100 mM $NaClO_4$ at 298 K were determined by spectrophotometric titration. The absorbance at equilibrium (A) is related to K_{an} by Equation (2), where, A_0 and A_∞ refer to the absorbance of the aqua complex [(η^6-arene)Ru(en)(H_2O)][PF_6]$_2$ (in the absence of Cl^-) and the chloro complex (formed from the aqua complex in the presence of 0.1 M NaCl), respectively.[16]

$$A = (A_0 + A_\infty K_{an}[Cl])/(1 + K[Cl]) \qquad (2)$$

Additions of NaCl were made giving chloride concentrations of 5–50 mM and the value of K_{an} was obtained by a computer fit to equation 2. The respective aquation equilibrium constants K_{aq} were calculated from the equation $K_{aq} = 1/K_{an}$, where K_{an} is the equilibrium constant corresponding to a chloride concentration which is the same as that of the initial aqua complexes.

Acknowledgments

We thank the Royal Society (the Royal Fellowship for F.W.), Edinburgh Technology Fund, CVCP (ORS Award for H.C.), EPSRC and EC COST D20 for support, Dr. John Parkinson for NMR advice, and Dr. Duncan Jodrell and colleagues in the CRUK Oncology Unit (Western General Hospital, Edinburgh) for stimulating discussions.

[1] R. E. Morris, R. E. Aird, P. del S. Murdoch, H. M. Chen, J. Cummings, N. D. Hughes, S. Parsons, A. Parkin, G. Boyd, D. I. Jodrell, P. J. Sadler, *J. Med. Chem.* **2001**, *44*, 3616–3621.
[2] R. E. Aird, J. Cummings, A. A. Ritchie, M. Muir, R. E. Morris, H. Chen, P. J. Sadler, D. I. Jodrell, *Br. J. Cancer* **2002**, *86*, 1652–1657.
[3] C. S. Allardyce, P. J. Dyson, D. J. Ellis, S. L. Heath, *Chem. Commun.* **2001**, 1396–1397.
[4] W. S. Sheldrick, S. Heeb, *Inorg. Chim. Acta* **1990**, *168*, 93–100.
[5] H. Chen, J. A. Parkinson, R. E. Morris, P. J. Sadler, *J. Am. Chem. Soc.* **2003**, *125*, 173–186.
[6] Z. J. Guo, P. J. Sadler, *Adv. Inorg. Chem.* **2000**, *49*, 183–306.
[7] F. Wang, H. Chen, J. A. Parkinson, P. d. S. Murdoch, P. J. Sadler, *Inorg. Chem.* **2002**, *41*, 4509–4523.
[8] A. C. G. Hotze, A. H. Velders, F. Ugozzoli, M. Biagini-Cingi, A. M. Manotti-Lanfredi, J. G. Haasnoot, J. Reedijk, *Inorg. Chem.* **2000**, *39*, 3838–3844.

[9] B. Lippert, C. J. L. Lock, B. Rosenberg, M. Zvagulis, *Inorg. Chem.* **1977**, *16*, 1525–1529.
[10] a) S. K. Mandal, A. R. Chakravarty, *Inorg. Chem.* **1993**, *32*, 3851–3854; b) D. L. Davies, J. Fawcett, S. A. Garratt, D. R. Russell, *Organometallics* **2001**, *20*, 3029–3034.
[11] W. J. Moore, *Physical Chemsitry*, 4th ed., Longmans, London, **1962**, p. 368.
[12] I. Rapaport, L. Helm, A. E. Merbach, P. Bernhard, A. Ludi, *Inorg. Chem.* **1988**, *27*, 873–879.
[13] M. Stebler-Rothlisberger, W. Hummel, P. A. Pittet, H. B. Burgi, A. Ludi, A. E. Merbach, *Inorg. Chem.* **1988**, *27*, 1358–1363.
[14] P. E. Dumas, E. E. Mercer, *Inorg. Chem.* **1972**, *11*, 531–535.
[15] F. Basolo, R. G. Pearson, *Mechanisms of Inorganic Reactions, A Study of Metal Complexes in Solution*, 2nd ed., Wiley, New York, **1967**, pp. 124–246.
[16] L. Dadci, H. Elias, U. Frey, A. Hornig, U. Koelle, A. E. Merbach, H. Paulus, J. S. Schneider, *Inorg. Chem.* **1995**, *34*, 306–315.
[17] a) J. A. Broomhead, F. Basolo, R. G. Pearson, *Inorg. Chem.* **1964**, *3*, 826–832; b) J. A. Broomhead, L. Kane-Maguire, *Inorg. Chem.* **1968**, *7*, 2519–2523; c) T. W. Hambley, G. A. Lawrance, *Aust. J. Chem.* **1984**, *37*, 435–441; d) L. A. P. Kane-Maguire, G. Thomas, *J. Chem. Soc. Dalton Trans.* **1975**, 1324–1329; e) C.-K. Poon, D. A. Isabirye, *J. Chem. Soc. Dalton Trans.* **1977**, 2115–2120.
[18] A. M. Sargeson, G. H. Seale, *Inorg. Chem.* **1967**, *6*, 2172–2180.
[19] H. Chen, J. A. Parkinson, S. Parsons, R. A. Coxall, R. O. Gould, P. J. Sadler, *J. Am. Chem. Soc.* **2002**, *124*, 3064–3082.
[20] E. van der Geer, A. Habtemariam, F. Wang, R. Fernández, M. Melchart, P. J. Sadler, unpublished results.
[21] a) T. Matsubara, C. Creutz, *J. Am. Chem. Soc.* **1978**, *100*, 6255–6257; b) T. Matsubara, C. Creutz, *Inorg. Chem.* **1979**, *18*, 1956–1966.
[22] J. A. Broomhead, L. Kane-Maguire, D. Wilson, *Inorg. Chem.* **1975**, *14*, 2575–2577.
[23] B. Bosnich, F. P. Dwyer, *Aust. J. Chem.* **1966**, *19*, 2235–2240.
[24] a) M. Jennerwein, P. A. Andrews, *Drug Metab. Dispos.* **1995**, *23*, 178–184; b) R. B. Martin in *Cisplatin Chemistry and Biochemistry of a Leading Anticancer Drug* (Ed.: B. Lippert), Wiley-VCH, Zurich, **1999**, pp. 183–205.
[25] M. J. Bloemink, J. Reedijk, *Met. Ions Biol. Syst.* ***1996***, 32, 641–685.
[26] G. M. Sheldrick, *SADABS.* Bruker-AXS, Madison, Wisconsin, USA, **1997.**
[27] R. H. Blessing, *Acta Crystallogr. Sect. A* **1995**, *51*, 33–38.
[28] P. T. Beurskens, G. Beurskens, W. P. Bosman, R. de Gelder, S. Garcia-Granda, R. O. Gould, R. Israel, J. M. M. Smits, The DIRDIF96 Program System, Technical Report of the Crystallography Laboratory, University of Nijmegen, The Netherlands, **1996**.
[29] G. M. Sheldrick, SHELXTL, Bruker-AXS, Madison, Wisconsin, USA, **1997**.
[30] A. L. Spek, *PLATON- A Multipurpose Crystallographic Tool*, Utrecht University, Utrecht, The Netherlands, **2002.** PC version: L. J. Farrugia, *J. Appl. Crystallogr.* **1999**, *32*, 837–838.
[31] F. H. Allen, O. Kennard, R. Taylor, *Acc. Chem. Res.* **1983**, *16*, 146–153.
[32] R. Sparks, GEMINI, Bruker-AXS, Madison, Wisconsin, USA, **1998**.
[33] R. I. Cooper, R. O. Gould, S. Parsons, D. J. Watkin, *J. Appl. Crystallogr.* **2002**, *35*, 168–174.
[34] D. J. Watkin, C. K. Prout, J. R. Carruthers, P. W. Betteridge, R. I. Cooper, CRYSTALS, **2001**, Issue 11, Chemical Crystallography Laboratory, Oxford, UK.

Received: January 10, 2003
Revised: August 4, 2003 [F4724]